Interface magnetic and optical anisotropy of ultrathin Co films grown on a vicinal Si substrate

A. Stupakiewicz,[1,2] A. Kirilyuk,[2] A. Fleurence,[3] R. Gieniusz,[1] T. Maroutian,[3] P. Beauvillain,[3] A. Maziewski,[1] and Th. Rasing[2]

[1]*Laboratory of Magnetism, University of Bialystok, Lipowa 41, 15-424 Bialystok, Poland*

[2]*Institute for Molecules and Materials, Radboud University Nijmegen, Heyendaalseweg 135, NL-6525 AJ Nijmegen, The Netherlands*

[3]*Institut d'Electronique Fondamentale, UMR CNRS 8622, Université Paris-Sud, 91405 Orsay, France*

(Received 6 May 2009; revised manuscript received 28 August 2009; published 29 September 2009)

Vicinal substrates provide unique opportunities to engineer the magnetic anisotropies of magnetic ultrathin films. Here we study Co layers on step-bunched Si(111) substrates, with or without a Cu interlayer, taken as model samples. To correlate their interface morphology with the step-induced magnetocrystalline anisotropy and the second-order optical polarization, the magnetization reversal, ferromagnetic resonance, and the interface-induced nonlinear magneto-optical spectroscopic response was investigated. We show that both the magnetic anisotropy of the Co layer and the nonlinear magneto-optical response are strongly modified by the addition of the Cu buffer. Thus, the Cu layer reduces the influence of step bunches on the in-plane anisotropy while simultaneously changing the uniaxial anisotropy constant. This is accompanied by a relative change in the rotational harmonics of the nonlinear optical signals that reflect the changes in the interface structure.

DOI: 10.1103/PhysRevB.80.094423 PACS number(s): 75.30.Gw, 42.65.Ky, 75.70.−i, 78.20.Ls

I. INTRODUCTION

In a crystalline solid, the symmetry breaking by the presence of a surface or an interface leads to a number of physical phenomena. This happens because of the interface-induced modification of the electron wave functions resulting in changes in the total energy as well as in the response of the system to external stimuli. As a consequence, in magnetism, the studies of surfaces and thin films have attracted a lot of fundamental interest and have lead to a continuously increasing number of applications.[1] Examples range from interlayer exchange coupling and giant magnetoresistance, to the read heads of hard drives, magnetic sensors, and magnetic random access memories.

One direct consequence of the presence of an interface is the modification of the magnetocrystalline anisotropy. This happens because the orbital motion of the electrons is strongly affected by the introduced symmetry breaking. It is then the asymmetry of the averaged orbital moments that defines the interface contribution to the magnetic anisotropy.[2] This contribution to the total magnetic anisotropy of the sample can easily be observed in ultrathin magnetic films, where the interface part becomes even dominating in some cases. As a consequence, a spin reorientation transition, from perpendicular to in-plane magnetization orientation, can be observed as a function of the thickness of the magnetic film, under/over layer thickness, morphology of the substrate etc.

Moreover, the anisotropy of the electron orbitals will also affect the optical response of the surface via changes in the selection rules for the optical transitions. This phenomenon, however, is difficult to observe in linear optical response, where the contribution from the underlying bulk is dominating. The situation changes drastically in the second-order optical response that is symmetry forbidden in the bulk of centrosymmetric materials and only appears at the surfaces and interfaces due to the symmetry breaking. Such magnetization-sensitive optical second-harmonic generation (MSHG) possesses a unique combination of extreme surface/interface sensitivity with giant magneto-optical effects[3] and is therefore particularly suitable for studies of interface-related magnetic phenomena.

Though exact mechanisms differ, there is a certain similarity (at least on a qualitative level) in the way how the changes in the orbital motion of electrons affect the magnetocrystalline anisotropy and the MSHG response. For example, the motion of electrons out of the surface plane (along z axis) is usually less restricted, leading to increased in-plane orbital moment values and strong modification of the magnetic anisotropy. Similarly, the zzz component of the nonlinear optical tensor will undergo strong changes because of this asymmetry in the electronic potential. The difference is that the magnetic anisotropy will also be modified in centrosymmetric systems, such as a single atomic monolayer, while for MSHG, lifting of this symmetry is essential.

In this work we study the interface- and step-induced modification of magnetic anisotropy in Co layers grown on step-bunched Si(111) substrates. Magneto-optical measurements in both polar and longitudinal configuration, angle-dependent ferromagnetic resonance, and MSHG are used to characterize the magnetic behavior of the samples. An attempt is made to correlate the influence of magnetic anisotropy with the rotational anisotropy of the MSHG signal. When a thin Cu layer is added between Si and Co, drastic change in the MSHG signals correlates with the absence of cobalt silicides in that case. This is also accompanied by a strong variation in the azimuthal dependence of the magnetic parameters and of the coercive field. The further in-depth development of this MSHG technique could therefore provide a sensitive method for external optical detection of magnetic anisotropies for morphology-induced changes in nanostructured materials. In addition we should note that possible resonance effects, such as due to the band gap of Si, or the consequence of surface-plasmon resonances in Au, both increase the total signal and allow for a clear separation of the various contributions to the total MSHG signal.

Below, Sec. II presents the sample preparation and the magnetic characterizations, including the derivation of the anisotropy constants. Section III deals with the nonlinear magneto-optical response from the structures, followed by discussion of the results in Sec. IV and conclusions in Sec. V.

II. STEPPED Si SUBSTRATES AND STEP-INDUCED ANISOTROPY OF Co FILMS

The structural morphology of substrates and/or interfaces plays a key role in their magnetic properties such as magnetic anisotropy,[4] spin reorientation transition,[5,6] magnetic domain structures,[7] etc. The controlled modification of the substrate morphology can be realized using vicinal nonmagnetic substrates providing a regular array of oriented steps with a precisely determined density.[8] The influence of steps on magnetic anisotropy can be treated as the appearance of periodic magnetic charges, leading to a dipolar in-plane anisotropy.[9] Thus, when the film is grown on a stepped surface, in addition to the usual magnetic shape and magnetocrystalline anisotropies, also in-plane uniaxial step-induced magnetic anisotropy should be taken into account.

Such extra anisotropy can favor magnetic-moment alignment either perpendicular[10] or parallel to the step edges.[11] Controlling the magnetocrystalline anisotropy energy and spin-orbit coupling by depositing vicinal Co films was reported in Ref. 12. The combination of cubic magnetocrystalline anisotropy with step-induced anisotropy was studied in Co films deposited on Cu(001) and Cu(111) substrates.[11,13,14]

One of the other possibilities to design the required surface morphology is via ion implantation. The surface reconstruction of an implanted vicinal Si(111) surface with both onefold and threefold symmetry was analyzed by reflective second-harmonic generation.[15] It has also been demonstrated that a modified Si surface imposes its symmetry on the metal layers deposited including thin buffer layers. The magnetic properties of ultrathin Co/Si films and the influence of Co silicide formation have been investigated in Ref. 16. Co films were shown to have strongly preferred growth along the step edges of the Si substrate.

A. Sample preparation

Our samples were deposited by molecular-beam epitaxy in an ultrahigh vacuum (UHV) chamber with a base pressure in the 10^{-10} mbar range. Substrates were *n*-doped Si(111) vicinal substrates with 2° misorientation toward the [11–2] direction and a resistivity of 0.01 Ω cm. Before metal growth the substrates are prepared under UHV conditions by heating up to 1250 °C by direct current.[17] The temperature is monitored using a thermocouple up to 550 °C and by an infrared pyrometer above this. For Si(111) misoriented toward [11–2], such preparation induces the formation of a step-bunches array on the surface oriented along the [−110] direction and separated by 7×7 reconstructed terraces[18] of about 80 nm length.[19]

Two types of samples were studied: without and with a 4 ML Cu buffer layer, deposited at 100 °C, before a 15 ML Co layer deposition at room temperature (RT). Below we shall denote these films as Co/Si and Co/Cu/Si structures. For the Co/Si structure we used 0.5 ML Au deposition at 440 °C in order to reconstruct the Si surface prior to Co deposition,[19] which does not have any influence on the physical properties of the sample. A schematic configuration of the samples is shown on Fig. 1. All metals are evaporated from resistive-heated crucibles. The thickness of the films and growth rates are measured by means of a quartz microbalance and are typically 0.8, 0.85, and 0.4 ML/min for gold, copper, and cobalt, respectively.

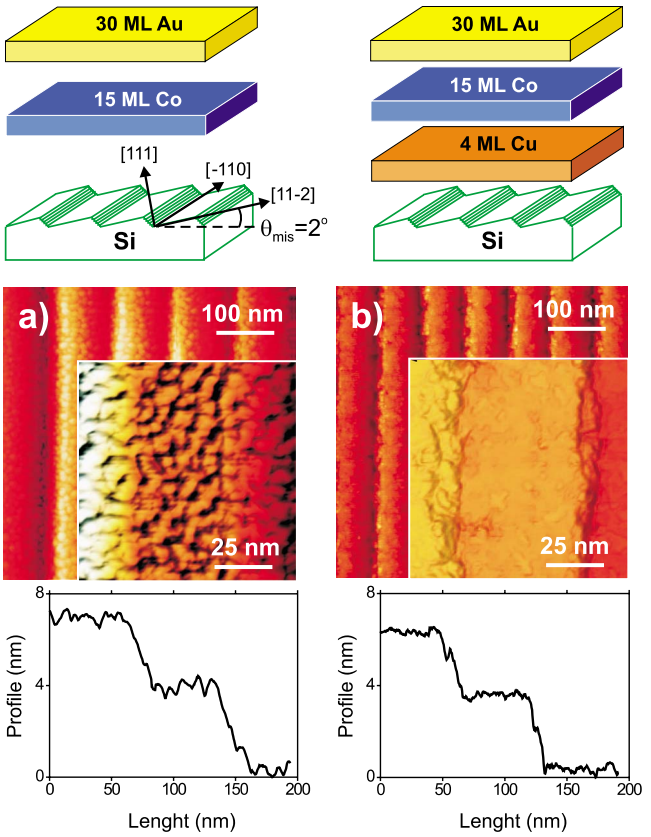

FIG. 1. (Color online) *In situ* STM images with different resolution of Co surfaces in the following structure: (a) 15 ML Co/Si, (b) 15 ML Co/Cu/Si. Top panels show the configuration of both samples including the Au protective layer.

The insertion of a Cu layer leads to the formation of a Cu silicide film that is expected to avoid the formation of a Co-silicide film when cobalt is deposited. Earlier investigations by second-harmonic generation[20] showed that the Cu coverage preserves the vicinal character of the Si substrate. The Cu silicide is not perfectly homogeneous on terraces with islands preferentially positioned on the top of the step bunches. The Co deposition onto bare Si(111) substrates, even at RT, gives rise to a silicide layer,[21,22] the composition and crystalline structure of which remains unclear and with a thickness varying in the 4–6 ML range.

After Co deposition, the surfaces of both samples were investigated *in situ* using scanning tunneling microscopy (STM) (Fig. 1). The stepped structure of both samples can be clearly seen. On each sample, on several areas of 30 ×500 nm^2 size, oriented on the terraces along the bunch direction (Si[−110]), the root-mean-square (rms) roughness

was calculated. The images in Fig. 1 indicate a uniform distribution and an rms roughness of 0.18 nm for Co/Si and 0.12 nm for Co/Cu/Si samples. This change in the roughness value may be due to the restructuring of the interface resulting from the Co-Si silicide formation. All the samples were afterwards capped with a 30 ML Au protective layer enabling an *ex situ* study.

B. Magnetization reversal from MOKE

The magnetization reversal process was studied with the magneto-optical Kerr effect (MOKE) using a diode laser at 640 nm, a photoelastic modulator, and employing a lock-in amplifier for the detection of the signal. All measurements were done at room temperature. A slightly focused laser beam illuminated the sample area with a diameter of about 0.5 mm. All three magnetization components could be measured either in the same geometry or with an appropriate adjustment of the angle of incidence. In most of the MOKE experiments discussed in this paper, magnetization hysteresis curves were recorded in the longitudinal MOKE (L-MOKE) geometry as a function of the sample azimuthal angle φ_H from 0° to 360° by 5° steps around the surface-normal direction, φ_H being measured with respect to the miscut direction (toward Si[11–2]). The angle of light incidence was kept at 50°. In addition, the polar magnetization component was measured using two different configurations: either polar MOKE geometry with close-to-normal incidence of the laser light, or after separation of the polar component from the L-MOKE measurement.[23]

A mainly in-plane magnetization state was observed from the MOKE loops measured for both samples. From the L-MOKE hysteresis curves, the coercive field H_c and the remanence magnetization M_r (calculated as the L-MOKE hysteresis loop amplitude in millidegree, at $H=0$) are derived as a function of the azimuthal angle φ_H. The results are plotted in Fig. 2 for both Co/Si and Co/Cu/Si samples. The insets show typical hysteresis loops measured for two samples at azimuthal angles $\varphi_H=0°$ and 90° (the in-plane magnetic field applied perpendicular and parallel to the Si[−110] direction). The opposite sign of the L-MOKE signal for the two samples can be explained by the uniaxial symmetry contribution and the interference between the optostructural (perturbation) tensor (induced by the stepped interface symmetry) and the usual magneto-optical tensor (from the nominal flat surface), see Ref. 24 for details. The influence of the steps on the magnetization reversal behavior is visible along with a strong modification of this behavior due to the presence of the Cu buffer layer. The azimuthal dependence of the L-MOKE remanence for the Au/Co/Si sample shows characteristic maxima at $\varphi_H=90°$ and 270° and smaller ones at $\varphi_H=0°$ and 180°, usual attributes of a uniaxial magnetic anisotropy. In contrast, in the case of the Co/Cu/Si sample, this uniaxial character becomes much less significant with easy axes rotating 90°, see Fig. 2. In general, a less distorted cubic structure may be expected for Co on a Cu(111) surface,[14] which is corroborated by the observation of a higher-symmetry pattern in Fig. 2 for this sample. Thus for the Co/Cu/Si sample we have the effect of a partial cubic symmetry on the magnetic switching behavior, like this would occur for a film with a threefold symmetry axis, and less-pronounced influence of the steps.

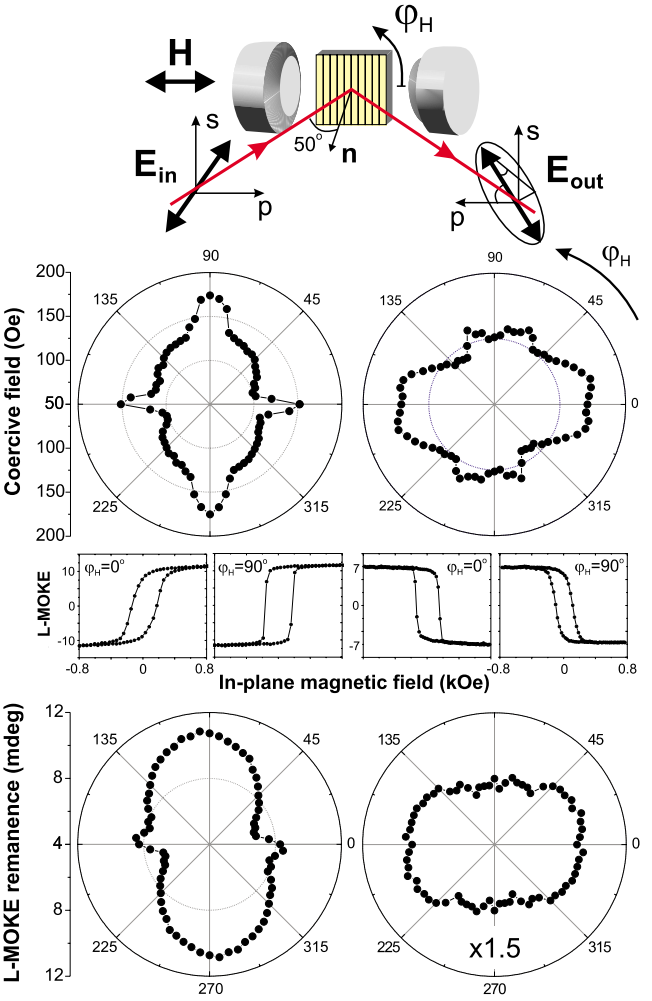

FIG. 2. (Color online) Azimuthal dependence of the remanence measured as L-MOKE ellipticity and coercivity field for Co/Si sample (left panels) and Co/Cu/Si sample (right panels). Hysteresis loops measured as L-MOKE ellipticity for $\varphi_H=0°$ and 90° are shown in the middle. Top panel shows the experimental L-MOKE geometry.

C. Magnetic anisotropy from FMR

Magnetic-anisotropy measurements were performed by means of a ferromagnetic resonance (FMR) X-band spectrometer at a frequency of 9.5 GHz. The measured resonance field H_r is related to the magnetic-anisotropy constants and enables determination of the easy magnetization axes appearing as minima in H_r.[25] An external magnetic field was applied to the sample in different directions, defined by the polar θ_H and azimuthal φ_H angles measured from the film normal and miscut direction in the sample plane, respectively, see inset in Fig. 3. For both samples the easy magnetization axis lies approximately in the sample plane, which follows from the measured dependencies $H_r(\theta_H)$ for various azimuthal angles φ_H. The dependencies of the H_r field on the

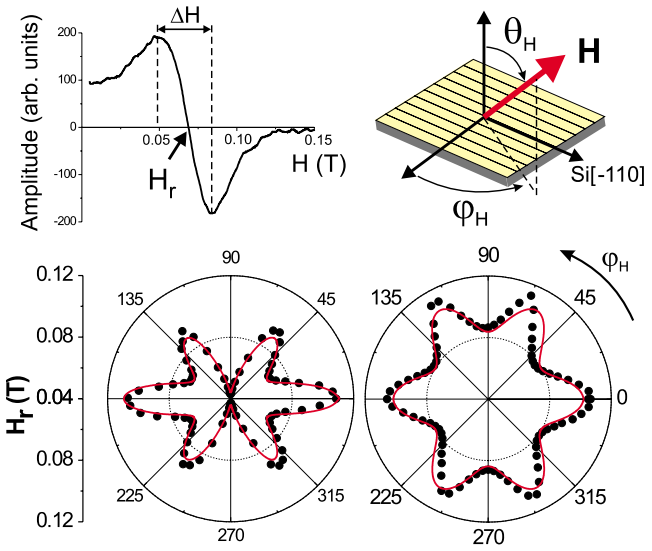

FIG. 3. (Color online) Experimental data of $H_r(\varphi_H)$ in-plane dependencies for Co/Si (left) and Co/Cu/Si (right) samples. Solid lines were fitted using the anisotropy constants from Table I. Top panels show the magnetic field orientation and an exemplary FMR line with similar value of the bandwidth ΔH for two samples.

angle φ_H for both samples are shown in Fig. 3. From these plots, the existence of a threefold anisotropy component in the film plane is easy to note. This result also correlates with the angular dependencies of the remanence and coercive fields, obtained from MOKE, as well as from the MSHG data below.

The easy magnetization axis was deduced by analyzing the $H_r(\theta_H, \varphi_H)$ dependencies. From the $H_r(\varphi_H)$ curve of the Co/Si sample, the easy magnetization directions are clearly visible to be near 90° and 270°—as a global minimum in the Si[−110] direction [see Fig. 3 (left)]. This corresponds therefore to the appearance of a step-induced uniaxial in-plane anisotropy that dominates for this sample. This result correlates well with the MOKE experiments (Fig. 2). In addition a sixfold symmetry of the pattern is visible, corresponding to the three easy axes in the film plane.

In contrast, in the case of the Co/Cu/Si sample the step-induced anisotropy is practically negligible and an almost ideal sixfold (cubic) symmetry is observed [Fig. 3 (right)]. In this case the 4 ML Cu covering Si appears to completely screen the effect of the uniaxial symmetry from the steps on the substrate. The results of the magnetic anisotropy from the FMR are thus in agreement with the MOKE data.

In our analysis of the experimental data, we have taken into consideration the following contributions: (i) the uniaxial anisotropy related to the miscut direction defined by

TABLE I. The magnetic anisotropy constants for different samples were determined using Eq. (1).

Sample	K_{u1} (MJ/m^3)	K_1 (MJ/m^3)	K_{vic} (MJ/m^3)
Au/Co/Si	0.23	0.16	−0.01
Au/Co/Cu/Si	0.41	0.13	0.002

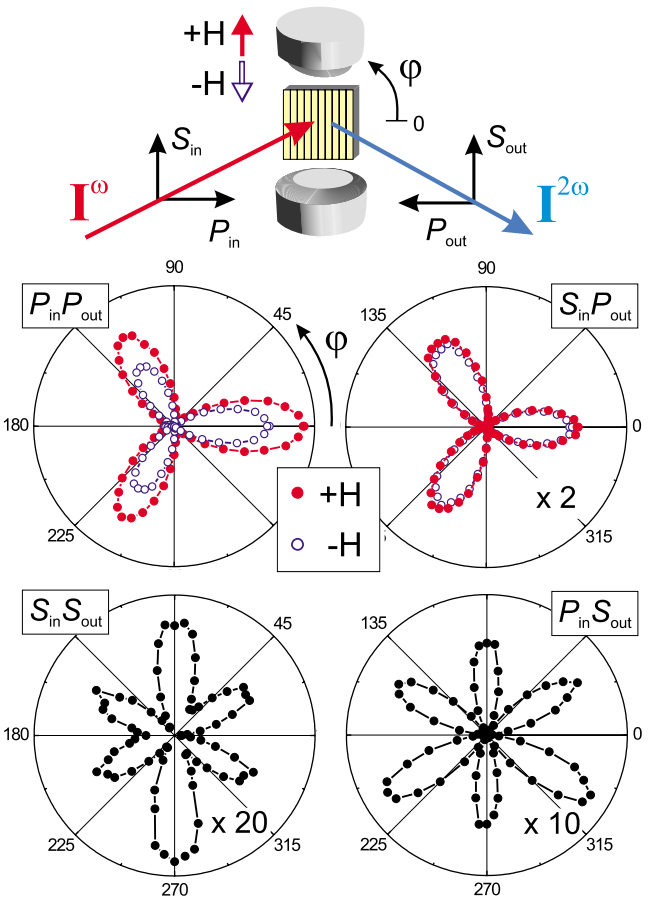

FIG. 4. (Color online) Azimuthal dependence of the MSHG intensity from the Co/Si sample for different polarization combinations (indicated in the figure) and 750 nm fundamental wavelength. The inset shows the experimental geometry as well as the definition of the incoming and outgoing light polarizations. Multiplication factors scaling the intensity data with respect to the $P_{in}P_{out}$ combination are shown in the plots. Magnetic field is applied in the film plane perpendicular to the plane of incidence (transverse geometry).

the unit vector[6] $\mathbf{v}_{mis}=(\sin\theta_{mis}, 0, \cos\theta_{mis})$ with $\theta_{mis}=2°$, (ii) the magnetic shape anisotropy, (iii) the step-induced uniaxial in-plane anisotropy, and (iv) the magnetocrystalline anisotropy.[1] The resulting expression is

$$E_A(\theta,\varphi) = K_{u1}[1-(\mathbf{m}\cdot\mathbf{v}_{mis})^2] - \frac{1}{2}\mu_0 M_s^2 \sin^2\theta + K_{vic}\sin^2\theta\sin^2\varphi + K_1\left(\frac{1}{4}\sin^4\theta + \frac{1}{3}\cos^4\theta - \frac{\sqrt{2}}{3}\sin^3\theta\cos\theta\sin 3\varphi\right), \quad (1)$$

where K_{u1} is the uniaxial perpendicular anisotropy constant, K_{vic} is the uniaxial in-plane step-induced anisotropy constant, K_1 is the first-order cubic magnetocrystalline constant, $\mathbf{m}=(\sin\theta\cos\varphi, \sin\theta\sin\varphi, \cos\theta)$ is the unit magnetization vector, θ is the angle between the magnetization direction and the sample plane normal, and φ is the angle of the in-plane magnetization orientation relative to the miscut direc-

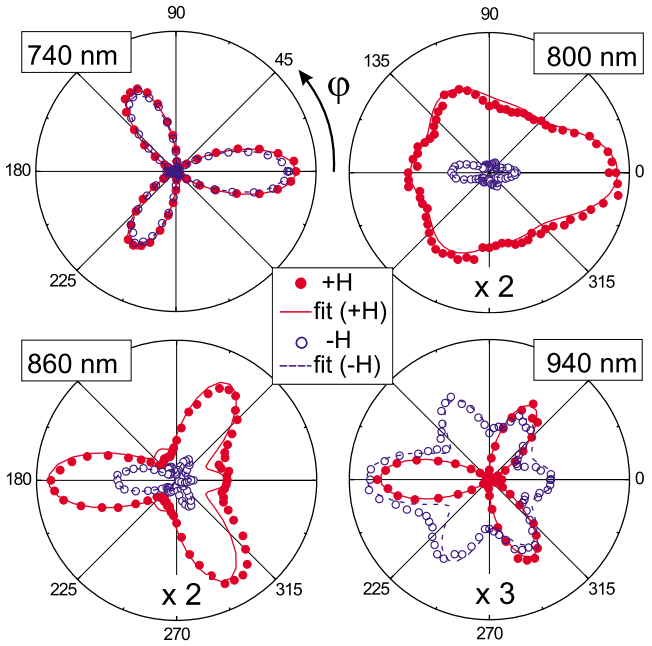

FIG. 5. (Color online) Rotational anisotropy patterns of the MSHG intensity from the Co/Si sample for the $P_{in}P_{out}$ polarization combination and for two different directions of the applied magnetic field, measured at different wavelengths of the fundamental light: (a) 740, (b) 800, (c) 860, and (d) 940 nm. Multiplication factors scaling the intensity data with respect to the 740 nm wavelength are shown in the plots.

tion. The fits using Eq. (1) and standard FMR conditions[25] for both samples are shown in Fig. 3 by solid lines. These fits obviously agree well with the experimental points and allowed us to derive the values for the magnetic anisotropy constants (see Table I). A strong reduction in the step-induced anisotropy constant due to the Cu buffer layer is obvious. In contrast, the uniaxial perpendicular anisotropy constant appeared to be twice as high in that case; this may be caused by the reduced interface roughness, see STM images of Fig. 1.

III. NONLINEAR MAGNETO-OPTICAL RESPONSE OF STEP-BUNCHED SAMPLES

A. Magnetization-induced second-harmonic generation technique

Though the first predictions of magnetization-induced effects in SHG (MSHG) were made long ago,[26–28] the field of nonlinear magneto-optics really evolved in the past decade only after the observation of huge magneto-optical effects from magnetic surfaces and interfaces.[29,30] The recent strong developments of nonlinear magneto-optics[3] are clearly related to the enormous interest in the study and applications of magnetic multilayers and nanostructures as well as to the development of solid-state mode-locked femtosecond lasers that are particularly suitable for these kinds of studies. Important achievements were the demonstration of the extreme sensitivity of MSHG to the slightest modifications of the transition-metal surfaces[30–32] and the possibility to measure the magnetization of a buried interface.[33]

MSHG results from the nonlinear polarizability of a medium excited by an incident light wave of frequency ω. The induced polarization serves as a source for the transmitted and reflected light. This polarization $\mathbf{P}$ can be written in the electric-dipole approximation as an expansion in powers of the optical electric field $\mathbf{E}(\omega)$,

$$\mathbf{P}(\omega,2\omega,\ldots) = \chi^{(1)}\mathbf{E}(\omega) + \chi^{(2)}\mathbf{E}(\omega)\mathbf{E}(\omega) + \cdots \qquad (2)$$

The tensor $\chi^{(1)}$ is the linear optical susceptibility allowed in all media. SHG is described by the second term with the corresponding nonlinear tensor $\chi^{(2)}$ allowed only in noncentrosymmetric media. Alternatively, $\chi^{(2)}$ is allowed at the symmetry-breaking surfaces or interfaces of a centrosymmetric medium. In the presence of a spontaneous or magnetic field induced magnetization $\mathbf{M}$, the nonlinear second-order optical polarization of an interface $\mathbf{P}^{nl}(2\omega)$ can be written as

$$\mathbf{P}^{nl}(2\omega) = \chi^{cr}\mathbf{E}(\omega)\mathbf{E}(\omega) + \chi^{magn}\mathbf{E}(\omega)\mathbf{E}(\omega)\mathbf{M}, \qquad (3)$$

where the first term describes the purely crystallographic contribution while the second one only exists in the presence of a magnetization $\mathbf{M}$ and describes MSHG. Note that $\mathbf{M}$ is an *axial* vector so that the inversion operation does not change its sign and the surface/interface sensitivity also holds for magnetic materials.

The number of nonzero components of $\chi^{(cr)}$ and $\chi^{(magn)}$ tensors depends on the crystallographic and magnetic symmetry of the interface.[3] In the case of low-symmetry interfaces, such as considered in this paper, the number of independent tensor components is large, so that it is impossible to separate their individual contributions to the total response. Nevertheless, as it has been demonstrated in Refs. 34–36 a set of $\chi^{(2)}$ elements for an interface with a particular (magnetic) symmetry results in a characteristic rotational anisotropy pattern. We will use such approach here, measuring the MSHG intensity as a function of magnetic field and azimuthal angle, and then separating the different rotational harmonics. A comparative study of the two samples will also allow, to some extent, to separate the contributions of different interfaces.

B. Experimental MSHG technique

The MSHG measurements were performed using a mode-locked Ti-sapphire (MaiTai, Spectra-Physics) femtosecond laser operating in the 740–940 nm range. The pulse width of the laser was 150 fs and the repetition rate 80 MHz. The laser beam was focused onto a 50-μm-diameter spot with average power about 35 mW. The SHG signal was measured using a photomultiplier after a special filtering to reject the fundamental wavelength. We applied an in-plane magnetic field of about 0.2 T in the transverse magneto-optical configuration which saturates the in-plane magnetization. The MSHG intensity measurements were done in the following four input-output polarization combinations: $P_{in}P_{out}$, $S_{in}P_{out}$, $P_{in}S_{out}$, and $S_{in}S_{out}$ (see Fig. 4), varying the azimuthal in-plane rotation angle of the sample from 0° to 360° by 5° steps around the surface-normal direction, and for each direction of the applied magnetic field, see inset in Fig. 4. Such sets of measurements thus allowed to separate the crystallo-

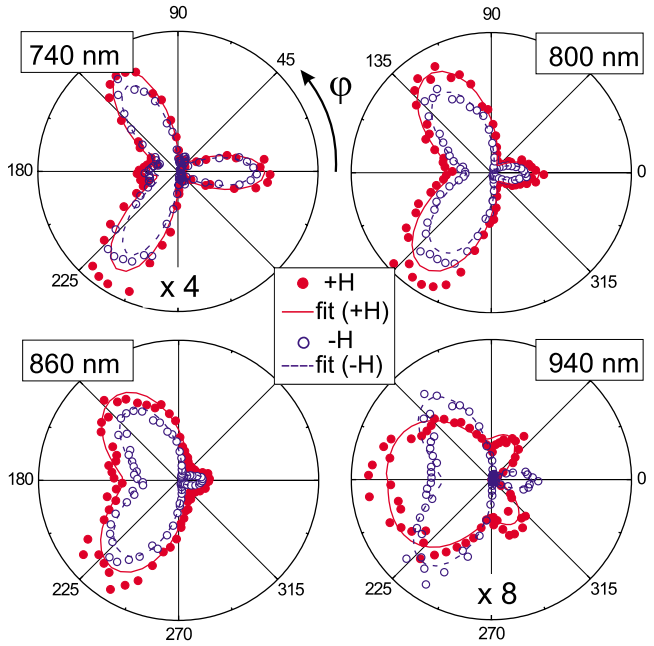

FIG. 6. (Color online) Rotational anisotropy patterns of the MSHG intensity from the Co/Cu/Si sample for the $P_{in}P_{out}$ polarization combination and for two different directions of the applied magnetic field, measured at different wavelengths of the fundamental light: (a) 740, (b) 800, (c) 860, and (d) 940 nm. Multiplication factors scaling the intensity data with respect to the 800 nm wavelength are shown in the plots.

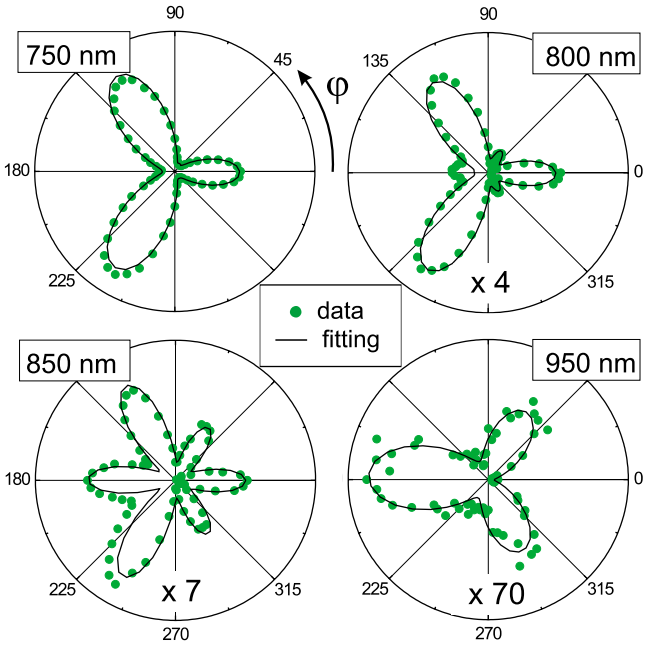

FIG. 7. (Color online) Rotational anisotropy patterns of the SHG intensity from the Si substrate for the $P_{in}P_{out}$ polarization combination, measured at different wavelengths of the fundamental light: (a) 750, (b) 800, (c) 850, and (d) 950 nm. Multiplication factors scaling the intensity data with respect to the 750 nm wavelength are shown in the plots.

graphic and magnetic contributions to the total signal.

Figure 4 shows examples of such MSHG rotational anisotropy patterns measured in all four polarization combinations for the Co/Si sample. These measurements were done at the fundamental wavelength of 750 nm, where the contribution of the Si substrate is dominating.[37] The basic $m3$ point-group symmetry of the Si(111) substrate is clearly seen in these patterns. Note the magnetization-induced change in the MSHG intensity in the $P_{in}P_{out}$ and the much smaller one in the $S_{in}P_{out}$ polarization combinations, that was absent (at all measured wavelengths) in other polarizations.

C. Optical anisotropy from MSHG

When the fundamental wavelength is changed to the low-energy part of spectrum, the influence of the Si substrate becomes much less dominating (see below), resulting, among other effects, in the observation of a stronger magnetic contrast, as Figs. 5 and 6 demonstrate. Furthermore, the influence of the miscut on the MSHG rotational anisotropy pattern is also much stronger at $\lambda > 800$ nm.

The third difference clearly visible in the MSHG rotational anisotropy patterns is the influence of the Cu interlayer, causing a strong difference between the patterns of Figs. 5 and 6. For comparison, Fig. 7 shows the SHG rotational anisotropy patterns measured from a bare Si substrate, for the same $P_{in}P_{out}$ polarization combination and for the same wavelengths. Note the strong reduction in the SHG intensity toward longer wavelengths, in agreement with earlier data.[37] Such reduction in the nonmagnetic background also explains the increase in the MSHG magnetic contrast in Figs. 5 and 6. On the other hand, the influence of step bunches is less visible on the data from Si than on those from the magnetic samples.

For a more quantitative discussion of the MSHG data, the curves of Figs. 5 and 6 were fitted with the following dependence

$$I_{2\omega}(\varphi, \pm \mathbf{M}) = |A_3 \sin(3\varphi + \varphi_3) + A_2 \sin(2\varphi + \varphi_2) + A_1 \sin(\varphi + \varphi_1) + A_0|^2. \quad (4)$$

The coefficients A_1, A_2, and A_3 (Refs. 20 and 34) obtained from these fits are plotted in Fig. 8 as a function of the fundamental wavelength. The phases φ_i used from fits within the whole wavelength range for each sample were separately fixed.

The following features should be noted from this figure: first of all, the dominating behavior of the A_3 coefficient at $\lambda < 800$ nm is clearly due to the influence of a bulklike SHG response from the Si(111) surface. In the same wavelength range, the second-order A_2 component is practically zero. Then, for both samples at $\lambda \geq 800$ nm the A_2 coefficient reveals a very strong magnetic dependence, even though its absolute value remains relatively small. Therefore this component can be assigned exclusively to the behavior of the Co layer interfaces. Note that the magnetization-induced effect is about three times larger for the Co/Si sample, probably due to the properties of the interface between the magnetic cobalt and nonmagnetic silicide. Next, we should note the different behavior of the threefold symmetric A_3 component at longer wavelengths: though its influence is much stronger

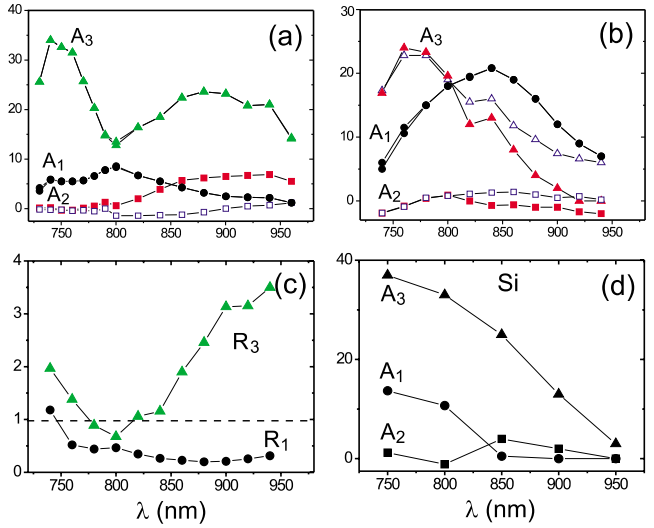

FIG. 8. (Color online) Spectral dependence of the MSHG reflectivity expressed as the various rotational harmonics coefficients A_3, A_2, and A_1 obtained from the fits of the rotational anisotropy data for $P_{in}P_{out}$ polarization combination measured from (a) Co/Si and (b) Co/Cu/Si samples, and (d) the Si substrate. Close and open points show the parameters derived from the data for magnetization up and down, respectively. (c) R_1 and R_3 are ratios of the A_1 and A_3 coefficients from the Co/Si and Co/Cu/Si samples, respectively.

in the Co/Si sample [see Fig. 8(c)], where it continues to be dominating, the magnetization-induced splitting only shows up in the presence of the Cu buffer layer. This underlines once again a considerable modification of the Co structure because of the silicide formation.

Moreover, the step-induced A_1 component is much more pronounced in the Cu-buffered sample and the ratio of this component for the two samples is decreased, as shown on Fig. 8(c). In neither of the samples, however, does this component show any magnetization dependence. It is therefore straightforward to attribute the pronounced behavior of this component to the nonmagnetic Cu/Si interface. For comparison, Fig. 8(d) shows the behavior of the same fitting parameters for the SHG signals measured from the bare step-bunched Si substrate. One can observe some qualitative similarity between the behavior of the threefold symmetry component A_3 from Si and from the Co/Cu/Si structure, between the component A_1 from Si and that from the Co/Si sample, and very low values of the A_2 contribution in all these three cases.

Note that we have not discussed the isotropic A_0 contribution, even though it shows both magnetic contrast and different spectral behavior for the two samples. The practical problem is that A_0, in contrast to the other contributions, originates from the out-of-plane components of the nonlinear optical tensor (predominantly the *zzz* one) and is thus not sensitive to the in-plane crystallographic symmetry. Therefore, it is present in the signal from all interfaces simultaneously and would only be separable in angle-of-incidence-dependent measurements.[33] However, such separation would be extremely challenging as well as rather ambiguous, taking into account the negligible thicknesses of our layers.

IV. DISCUSSION: A CORRELATION BETWEEN INTERFACE MORPHOLOGY, MAGNETIC ANISOTROPY, AND MSHG RESPONSE

Let us discuss, step-by-step, the properties of the individual layers and interfaces in a comparative way and their influence on the magnetic anisotropy of the structures as well as on the MSHG response generated by them. Note, first of all, that the MSHG response at shorter wavelengths ($<$800 nm) is dominated by the bulklike response of Si that occurs because of the onset of optical transitions at the second-harmonic frequency.[37] Because of the accompanying absorption, also the SHG intensity from the overlayers is reduced. A support of this is the absence of magnetic contrast for this wavelength range for all A coefficients of the two samples. The fingerprint of the response from the magnetic layers thus comes in the long-wavelength region where the influence of Si becomes negligible. In the following, we will therefore concentrate on the range above 800 nm fundamental wavelength.

The crucial difference between the two samples is the presence of the Cu buffer layer in the second one that prevents to a large extent the contact between the magnetic Co layer and the Si substrate. Instead, this results in the formation of two relatively sharp Cu/Si and Co/Cu interfaces, as compared to the alloyed transition silicide interlayer $Co/CoSi_x/Si$ of the Co/Si system. However, for the Cu case, the contact of the magnetic Co layer with the step-bunched Si surface is strongly reduced. Therefore, the introduction of the Cu layer changes the competition between the step-induced in-plane uniaxial and cubic bulklike magnetocrystalline anisotropies in favor of the latter. This is evidenced by the fivefold decrease in the step-induced anisotropy constant K_{vic} while the cubic one K_1 practically remains unchanged (see Table I).

On the other hand, the sharpness of the Cu/Si interface and the preservation of the step bunches reveal themselves in the strong first-order A_1 contribution to the MSHG. The growth of Cu on Si results in a Cu(111) layer,[14] this fact determining the magnetic anisotropy of the Co/Cu interface. As a result, magnetic contrast in the third-order MSHG magnetic A_3 coefficient is observed, which is absent in the signal from the Co/Si sample. This smooth Co/Cu interface, in addition, makes a contribution to the uniaxial out-of-plane anisotropy described by the K_{u1} constant, which is twice larger in the Co/Cu/Si sample as compared to the Co/Si one. If we assume, as one usually does for ultrathin Co films,[1] that this out-of-plane anisotropy is due to the interfaces only, and that the volume part is the same in the two cases, about a fivefold difference in the surface part between the two samples is obtained.

When Co is deposited on Si directly, cobalt silicide grows in a structure, that is, incompatible with the Si(111) structure. This results in an increase in the interface roughness and therefore increased contribution of this interface to the total MSHG signal. This is detected as the appearance of a strong magnetic signal in the second-order (A_2) contribution; the increase in this symmetry as compared to that of the steps (first-order A_1) may be explained by a multiple-twinning process.

In the case of the Co/Si sample, the deposition of the gold overlayer results in a large nonmagnetic threefold (A_3) MSHG contribution at wavelengths >800 nm. This can be explained by two coexisting mechanisms: (i) the gold layer apparently keeps the original (111) texture, which is thus probably true for both samples; (ii) due to the relatively large roughness (see STM images in Fig. 1) the SHG signal in this wavelength range may be amplified via plasmonic effects. Such amplification is considerably lower for the smooth surface of the Co/Cu/Si sample.

Thus, we are able to present a qualitatively coherent picture by means of a comparative treatment of the magnetic anisotropy and MSHG data. In the latter, the contribution of the Si(111) step-bunched substrate could be excluded thanks to a strong spectral dependence of the nonlinear optical signals. The different harmonics of the MSHG rotational anisotropy could be related, though in a not very direct way, to the various interfaces of the structures. The properties of these interfaces, then, are connected to the particular values of the magnetic anisotropy constants. One clear difference that is obvious from the rotational patterns of the resonance field and MSHG intensity is that while the magnetic anisotropy has a uniaxial character, the MSHG intensity rather reveals a unidirectional behavior. This is easy to understand if one realizes that for the MSHG process to occur, asymmetry between "up" and "down" is required, while this is not the case for the interface contribution to the magnetic anisotropy. Thus, a single isotropic monolayer may lead to a strong contribution to the magnetic anisotropy but not to a nonlinear optical response.

V. CONCLUSIONS

The results discussed in this paper serve two purposes. On the one hand, we have succeeded to establish, even though on a rather qualitative level, the correlation between magnetic interface anisotropy and the behavior of the nonlinear magneto-optical response. Thus, the presence of the *n*th-order component in the MSHG rotational anisotropy patterns indicates the existence of magnetic anisotropy of the same order. Therefore MSHG, in addition to its enhanced sensitivity to the magnetization of buried interfaces,[3] may also serve as a tool to detect the interface magnetic anisotropies. Theoretical work will be required to establish more quantitative links between these phenomena for further development of the MSHG technique.

On the other hand, this study was applied to a particular system of Co film grown on a vicinal Si(111) surface and thus provided exact data on the interface anisotropy of the Co/Si interface and its strong modifications by the insertion of a ultrathin Cu buffer. While silicide formation preserves step-induced in-plane anisotropy, the inserted Cu layer creates (111) texture and thus leads to an increase in both in-plane and out-of-plane uniaxial anisotropies. This behavior is clearly seen from the MSHG response and directly confirmed by MOKE and FMR measurements. We proposed a phenomenological model, for magnetic anisotropy description, includes uniaxial (perpendicular and in-plane) and cubic contributions, and also a geometrical factor originating from the vicinal substrates.

The understanding of the interface anisotropy in ultrathin film systems can be used to create new artificial systems with desired magnetic properties and reduced dimension down to atomic scale. Particularly interesting are combined nanostructured metallic magnetic systems with semiconducting vicinal substrates that may be the key to create spintronic devices as well as patterned or self-organized magnetic media (see e.g., Ref. 38). Moreover, the modifications of the magneto-optical properties in such materials can lead to the controllable localized surface-plasmon resonances. Therefore, the development of a versatile noninvasive magnetic characterization technique is an important milestone in the development of such nanostructures.

ACKNOWLEDGMENTS

This work was supported in part by European Community's Seventh Framework Programme (FP7/2007-2013) under Grant Agreement No. 214810 (FANTOMAS), the Dutch NanoNed initiative and the Polish Scientific Network ARTMAG.

[1] *Ultrathin Magnetic Structures I-IV*, edited by J. A. C. Bland and B. Heinrich (Springer, Berlin, 1994).
[2] P. Bruno, Phys. Rev. B **39**, 865 (1989).
[3] A. Kirilyuk and Th. Rasing, J. Opt. Soc. Am. B **22**, 148 (2005).
[4] P. Gambardella, A. Dallmeyer, K. Maiti, M. C. Malagoli, W. Eberhardt, K. Kern, and C. Carbone, Nature (London) **416**, 301 (2002).
[5] G. Rodary, V. Repain, R. L. Stamps, Y. Girard, S. Rohart, A. Tejeda, and S. Rousset, Phys. Rev. B **75**, 184415 (2007).
[6] A. Stupakiewicz, A. Maziewski, K. Matlak, N. Spiridis, M. Ślęzak, T. Ślęzak, M. Zając, and J. Korecki, Phys. Rev. Lett. **101**, 217202 (2008).
[7] Y. L. Iunin, Y. P. Kabanov, V. I. Nikitenko, X. M. Cheng, D. Clarke, O. A. Tretiakov, O. Tchernyshyov, A. J. Shapiro, R. D. Shull, and C. L. Chien, Phys. Rev. Lett. **98**, 117204 (2007).
[8] F. Leroy, P. Müller, J. J. Métois, and O. Pierre-Louis, Phys. Rev. B **76**, 045402 (2007).
[9] C. A. F. Vaz, S. J. Steinmuller, and J. A. C. Bland, Phys. Rev. B **75**, 132402 (2007).
[10] A. Stupakiewicz, A. Maziewski, M. Ślęzak, T. Ślęzak, M. Zając, K. Matlak, and J. Korecki, J. Appl. Phys. **103**, 07B520 (2008).
[11] R. K. Kawakami, M. O. Bowen, H. J. Choi, E. J. Escorcia-Aparicio, and Z. Q. Qiu, Phys. Rev. B **58**, R5924 (1998).
[12] S. S. Dhesi, G. van der Laan, E. Dudzik, and A. B. Shick, Phys. Rev. Lett. **87**, 067201 (2001).
[13] M. Cinal and A. Umerski, Phys. Rev. B **73**, 184423 (2006).
[14] M. Farle, W. Platow, E. Kosubek, and K. Baberschke, Surf. Sci. **439**, 146 (1999), and references therein.
[15] K. Y. Lo and Y. J. Huang, Phys. Rev. B **76**, 035302 (2007).
[16] H. Xu, A. C. H. Chuang, A. T. S. Wee, and D. M. Tong, Solid

State Commun. **126**, 659 (2003).
[17] A. Martinez-Gil, A. Rota, T. Maroutian, B. Bartenlian, P. Beauvillain, E. Moyen, and M. Hanbücken, Superlattices Microstruct. **36**, 235 (2004).
[18] F. K. Men, F. Liu, P. J. Wang, C. H. Chen, D. L. Cheng, J. L. Lin, and F. J. Himpsel, Phys. Rev. Lett. **88**, 096105 (2002).
[19] A. Rota, A. Martinez-Gil, G. Agnus, E. Moyen, T. Maroutian, B. Bartenlian, R. Mégy, M. Hanbücken, and P. Beauvillain, Surf. Sci. **600**, 1207 (2006).
[20] W. Cheikh-Rouhou, L. C. Sampaio, B. Bartenlian, P. Beauvillain, A. Brun, J. Ferré, P. Georges, J. P. Jamet, V. Mathet, and A. Stupakiewicz, Appl. Phys. B: Lasers Opt. **74**, 665 (2002).
[21] P. Luches, A. Rota, S. Valeri, I. I. Pronin, D. A. Valdaitsev, N. S. Faradzhev, and M. V. Gomoyunova, Surf. Sci. **511**, 303 (2002).
[22] C. Pirri, J. C. Peruchetti, G. Gewinner, and J. Derrien, Phys. Rev. B **29**, 3391 (1984).
[23] H. F. Ding, S. Pütter, H. P. Oepen, and J. Kirschner, J. Magn. Magn. Mater. **212**, 5 (2000).
[24] J. Hamrle, J. Ferré, J. P. Jamet, V. Repain, G. Baudot, and S. Rousset, Phys. Rev. B **67**, 155411 (2003).
[25] M. Farle, Rep. Prog. Phys. **61**, 755 (1998).
[26] P. S. Pershan, Phys. Rev. **130**, 919 (1963).
[27] R.-P. Pan, H. D. Wei, and Y. R. Shen, Phys. Rev. B **39**, 1229 (1989).
[28] W. Hübner and K. H. Bennemann, Phys. Rev. B **40**, 5973 (1989).
[29] J. Reif, J. C. Zink, C. M. Schneider, and J. Kirschner, Phys. Rev. Lett. **67**, 2878 (1991).
[30] H. A. Wierenga, W. de Jong, M. W. J. Prins, Th. Rasing, R. Vollmer, A. Kirilyuk, H. Schwabe, and J. Kirschner, Phys. Rev. Lett. **74**, 1462 (1995).
[31] M. Straub, R. Vollmer, and J. Kirschner, Phys. Rev. Lett. **77**, 743 (1996).
[32] Q. Y. Jin, H. Regensburger, R. Vollmer, and J. Kirschner, Phys. Rev. Lett. **80**, 4056 (1998).
[33] A. Kirilyuk, Th. Rasing, M. A. M. Haast, and J. C. Lodder, Appl. Phys. Lett. **72**, 2331 (1998).
[34] V. N. Gridnev, V. V. Pavlov, R. V. Pisarev, A. Kirilyuk, and Th. Rasing, Phys. Rev. B **63**, 184407 (2001).
[35] K. Sato, A. Kodama, M. Miyamoto, A. V. Petukhov, K. Takanashi, S. Mitani, H. Fujimori, A. Kirilyuk, and Th. Rasing, Phys. Rev. B **64**, 184427 (2001).
[36] L. Carroll, K. Fleischer, J. P. Cunniffe, and J. F. McGilp, J. Phys.: Condens. Matter **20**, 265002 (2008).
[37] S. A. Mitchell, J. Phys. Chem. B **107**, 9388 (2003).
[38] E. Moyen, M. Macé, G. Agnus, A. Fleurence, T. Maroutian, F. Houzé, A. Stupakiewicz, L. Masson, B. Bartenlian, W. Wulfhekel, P. Beauvillain, and M. Hanbücken, Appl. Phys. Lett. **94**, 233101 (2009).